RSC Advances

ROYAL SOCIETY OF CHEMISTRY

PAPER

View Article Online
View Journal | View Issue

Cite this: *RSC Adv.*, 2026, **16**, 15963

Characterisation and properties of metahalloysite-based geopolymer composites with micro/nano-Fe_3O_4 contents: effect of the mixing procedure

Rodrigue Cyriaque Kaze, *[abc] Joël Donkeng-Dazie, [a] Abdolhossein Naghizadeh[b] and Mohend Chaouche[c]

In this study, the effects of micro- and nano-sized iron powders, as well as the mixing procedure, on the fresh and hardened properties of metahalloysite-based geopolymer composites were investigated. Iron powders were incorporated at dosages of 2, 4, and 6 wt% of the binder, and two distinct mixing procedures were adopted for specimen preparation. In the first procedure, metahalloysite was dry-blended with the iron powder prior to the addition of the alkaline activator. In the second procedure, the iron powder was first dispersed in the alkaline solution, after which metahalloysite was gradually introduced into the mixture. Afterwards, the resulting paste samples were subjected to mechanical properties evaluation. Furthermore, both the raw materials and the synthesised binders were characterised in terms of phase composition and microstructure using Fourier-transform infrared spectroscopy (FTIR), X-ray diffraction (XRD), and scanning electron microscopy (SEM). The results indicated that compressive strengths of 55 and 58 MPa were achieved with the addition of 2 wt% nano-sized and 6 wt% micro-sized iron powder, respectively, when the first mixing procedure was applied. In contrast, for the second procedure, compressive strengths of 55 and 56 MPa were obtained at the corresponding iron powder contents. Overall, the findings suggest that nano-sized iron powder can effectively enhance the mechanical performance of geopolymer composites. The relatively high strength observed in specimens incorporating micro-sized iron powder is attributed to a filler effect that promotes pore refinement and results in a more compact, denser microstructure. Conversely, pre-dissolution of iron powder in the alkaline solution prior to the addition of metahalloysite was found to hinder the geopolymerisation reaction and the development of a well-connected geopolymer network, resulting in reduced compressive strength.

Received 9th February 2026
Accepted 16th March 2026

DOI: 10.1039/d6ra01146b

rsc.li/rsc-advances

1. Introduction

Geopolymer binder, an alternative to Portland cement, is formed from a mixture of an aluminosilicate powder and an acidic or alkaline solution at moderate temperatures.[1] Compared with conventional Portland cement, geopolymer binders exhibit a lower carbon footprint, enhanced durability under harsh conditions (*e.g.*, saline and acidic environments), and potentially higher mechanical strength, depending on the chemical and mineralogical composition of the solid precursor. Moreover, recent studies have reported the superior recyclability of geopolymer binders compared with Portland cement.[2–4] Their structure is primarily composed of Al–O–Si bonds, with Na^+ or K^+ cations balancing the negative charge within the aluminosilicate framework.[5] Commonly used aluminosilicate precursors for geopolymer production include metakaolin (derived from the thermal activation of kaolin), fly ash, blast-furnace slag, construction and demolition waste, and volcanic ash.[6] Recently, the use of metahalloysite, produced by the thermal activation of halloysite at temperatures between 550 and 850 °C, has attracted significant research interest.[7,8] This interest is primarily attributed to its excellent mechanical performance and favourable microstructural stability under both alkaline and acidic conditions.

The previous studies on metahalloysite-based geopolymer in the literature have mostly focused on the mix proportion,[9–11] varied heating temperature ranging between 450 and 850 °C,[12] curing temperature range of 20–80 °C,[13] concentration of alkaline[14,15] or acidic[16,17] solutions. Several studies have reported that employing the optimal temperature of 750 °C resulted in better performance.[7,8,18] Recent developments in nanomaterials have made the use of such materials in enhancing geopolymer's

[a]*School of Chemical Engineering and Mineral Industries (EGCIM), Department of Material Engineering, University of Ngaoundéré, P. O. Box 454, Ngaoundéré, Cameroon. E-mail: kazerodrigue@gmail.com*

[b]*Department of Engineering Sciences, University of the Free State, Bloemfontein, 9300, South Africa*

[c]*Université Paris-Saclay, CentraleSupélec, ENS Paris-Saclay, CNRS, LMPS – Laboratoire de Mécanique Paris-Saclay, 91190, Gif-sur-Yvette, France*

Table 1 The summary of the effects of iron powders on properties of hardened geopolymers, as reviewed from the literature

Raw materials	Iron source	Activator	Curing regime	Obtained results
Metakaolin[33]	Ferric ions solution (10, 20, 30, 40 and 50 mL)	Sodium silicate	Room temperature	71.59 MPa was achieved using 13.2 mL of Fe^{3+} and 20 mL of sodium silicate
Metakaolin[34]	Ferric ions (5, 10, 15 and 20 g)	Sodium silicate	Room temperature	72.80 MPa was attained by replacing the metakaolin with 5 g of ferric ions
Volcanic tuff[35]	Iron powder (IPW) waste at percentages of 5%, 10%, and 20%	Sodium silicate gel (SS) with SiO_2 and Na_2O contents of 28.8% and 14.2%	Two curing time temperatures of 25 °C and 80 °C for 24 h	The use of iron powder reduces the compressive strength by a percentage of 2.82%, 2.01%, and 22.479% for samples blended with 5, 10 and 20% IPW cured at 25 °C and, 49.79%, 30.84%, and 47.37% for those cured at 80 °C
Metakaolin[36]	Hematite, magnetite and goethite (5, 10 and 20 of each iron mineral)	Sodium silicate	Room temperature	55 MPa achieved on samples with 10% of hematite
Waste fired clay brick and metakaolin[37]	Hematite and rice husk ash (0 and 10 wt%)	Sodium silicate ($M_s = 1.6$)	Room temperature	For the metakaolin-based geopolymers the compressive strength increased from 53.34 to 69.08 MPa when the Fe_2O_3/SiO_2 increased from 0 to 0.8 Those of geopolymer materials derived from waste fired clay brick decreased from 45.42 to 21.15 MPa when their Fe_2O_3/SiO_2 molar ratios rise from 0 to 0.6 increases from 21.15 to 24.11 MPa beyond 0.6
Metakolin[32]	Hematite, magnetite and raw iron powders (2, 5, 10 and 20%)	Sodium silicate ($M_s = 1.5$)	20 °C	5% of hematite and raw iron gave the highest strength 65 MPa whereas no any increases was observed on samples blended with raw iron powder
Fly ash[38]	Waste iron powder (10 and 20%)	Sodium silicate	Room temperature	62.79 MPa achieved on sample blended with 20% of waste iron powder
High calcium fly ash[39]	Waste iron powder (5, 10, 15 and 20%)	Sodium silicate	Oven curing between 30 °C and 60 °C for 24 h	20% of iron powder ensured the highest strength of 50.5 MPa, which was approximately 76% of the strength of the control
Kaolin-zeolite[40]	Micro Fe_2O_3 (4, 6, and 8%)	NaOH-based activator containing 15% Na (Na/binder) by weight	Cured at 110 °C for 24 h using a furnace	Kaolin based geopolymer blended with 8% of micro iron powder was 5% higher than sample reference
Fly ash[41]	Iron ore tailing (10, 20 and 30%)	Sodium silicate	20 ± 2 °C and 90 ± 5% relative humidity	50 MPa achieved on sample blended with 20% of iron ore tailing
Slag[42]	Hematite (5, 10 and 15%)	Sodium silicate ($M_s = 1.8$)	Oven cured at 60 °C for 8 h	Replacing slag with hematite decreased the compressive strength from 73.6 to 32.46 MPa
Slag[43]	Iron filling (IF) obtained from iron local mechanical workshops (10, 20, 30, 40 and 50 wt%)	Sodium silicate ($M_s = 2$)	Room temperature	10% IF replacement ratio showed the highest values of 39 and 6.2 MPa for compressive and flexural strength with an increase of 12.1% and 25.5%

Table 1 (*Contd.*)

Raw materials	Iron source	Activator	Curing regime	Obtained results
				respectively compared to the control mixture
Volcanic ash[44]	0, 5, 10, 15, and 20% iron waste powder residues from a welding shop on the properties of PIPs	H_3PO_4 (6 M)	Room temperature	Iron powders can be used as a pore-forming agent as observed in the decrease of compressive strength from 28 to 2 MPa

mechanical and microstructural properties.[19] Various nanoparticles such as carbon nanotubes (CNTs), nano-silica, and nano-alumina have been widely incorporated into polymer and geopolymer composites to enhance mechanical performance, durability, and microstructural stability. These nanomaterials can improve matrix densification, crack resistance, and interfacial bonding within the composite structure.[20–23]

Some studies showed that the early and later age strengths of geopolymer pastes,[24] mortars, and concretes[25] improved when a small amount of nanomaterial powder, such as nano silica, alumina, or iron, was used. The reported effect of nanomaterials was attributed to accelerated cement hydration[26] and pozzolanic reaction,[26] reduced pores,[27] and enhanced interface bonding between binder phase and aggregates.[28] For example, Mohamed *et al.*[24] reported that the inclusion of nano rutile or anatase powders in mixtures increased the 28-day flexural strength of metahalloysite-based geopolymer pastes.

Nongnuang *et al.*[29] observed an improvement in the mechanical properties of a high-calcium fly ash-based geopolymer due to inclusion of up to 20 wt% waste iron powder (WIP) in the mixtures. It was reported that fly ash-based geopolymer binder containing 20 wt% WIP gave 28-day flexural strength of 8.5 MPa, which was almost three times higher than the reference mixture that was made without WIP addition. Khouadjia *et al.*[30] investigated the rheological behaviour and mechanical properties of volcanic tuff-based geopolymer blended with WIP up to 20 wt%. Results revealed that air content in the binder matrix increased to 3.5% with 20% iron powder (IP) substitution, accompanied by a slight rise in flow time (0.8–2 s). While the compressive strength and flexural strengths at 25 °C decreased by up to 22.48% and 28.39%, respectively. However, the compressive and flexural strengths almost doubled when the samples were oven-cured at 80 °C. Prałat *et al.*[31] evaluated the thermal parameters of geopolymer products modified with IP. They reported that introducing IP led to significant changes in their thermal properties, including thermal conductivity, specific heat, and thermal diffusivity. Wu *et al.*[32] produced Fe-based geopolymers by adding hematite (HE), magnetite (MA), and reduced iron powder (RIP) into metakaolin powder (MK) up to 20 wt% and evaluated their influence. They reported that RIP did not significantly reduce the strength of the geopolymer, maintaining performance close to that of the reference (geopolymer without additive), compared with HE and MA additives. Table 1 provides a summary of the parameters influencing the end properties of geopolymer blended with different iron mineral sources, as reviewed in the literature. All of these reviewed experiments include substituting precursor materials with iron minerals from various sources and then adding an alkaline solution activator to assess their effect on geopolymer characteristics. The unique aspect of this work is that it assesses the influence of mixing in order to understand the behavior of ferrous minerals in the geopolymer matrix. This would contribute to the literature on the role of minerals in the synthesis of geopolymers.

In the majority of previously reported studies, iron powder was incorporated by direct blending with solid precursors, without systematically considering the effects of particle size or the dispersion of iron powder in the alkaline activator. In contrast, the present study uniquely combines and compares two distinct incorporation approaches: (i) partial substitution of metahalloysite with micro- and nano-sized iron powders at levels of 0, 2, 4, and 6 wt%, and (ii) pre-dispersion of iron powder in the alkaline solution prior to the addition of the solid precursor. This dual approach enables a systematic evaluation of the influence of both particle size and mixing procedure on the fresh and hardened properties of metahalloysite-based geopolymer composites. Furthermore, the study focuses on the effects of iron powders on the setting time and later age (28 days) strengths of geopolymer mixtures, using iron powders composed of micro- and nano-particles in comparison. As iron particles are very fine and tend to agglomerate due to strong surface interactions, the effects of dispersion methods for iron powders were also investigated by dissolving the powders in an alkaline solution before introducing them into metahalloysite powder. In addition to compressive strength and setting time, the flowability of the mixtures was also studied and compared. The study provides information for systematic analyses on: (i) the effect of iron powder content, (ii) the effect of particle size of the iron powder, and (iii) the effect of dispersion methods on the properties of metahalloysite-based geopolymer binders.

2. Experimental program

2.1. Materials and geopolymer synthesis

Metahalloysite powder used as the main solid precursor for the geopolymer production, thermal halloysite clay at 700 °C, previously characterised by Kaze *et al.*[7] The alkaline solution was prepared by mixing 10 M NaOH with a commercial sodium silicate at a mass ratio of 1 : 2, as selected from a previous study.[7] Two types of iron powders were used: micro and nano, with particle diameters of −200 mesh (74 μm) and 50 nm,

Table 2 Mixing procedure of geopolymer binders

ID	Calcined halloysite (g)	Micro or nano iron powder (g)	Alkaline solution (g)
GMPH0	100	0	80
GPMH2	98	2	80
GPMH4	96	4	80
GPMH6	94	6	80

respectively. These iron powders were supplied by Alfa Aesar (micro iron powder) and Nanofer Star (nano iron powder). Two mixing procedures were employed for the synthesis of the geopolymer composites. In the first procedure, metahalloysite was dry-mixed with 2, 4, and 6 wt% iron powder, after which the alkaline activator was added at a solid-to-liquid ratio of 0.8. The mixture was then mechanically stirred at 1000 rpm for 3 min. The selected solid-to-liquid ratio was determined through preliminary trial mixes to achieve adequate workability of the fresh geopolymer paste. In the second mixing procedure, different iron powders were mixed with an alkaline solution for 30 seconds before adding the metahalloysite powder. Both procedures produced fresh geopolymer composite pastes, which were poured into 20 mm cubic moulds, and stored in room temperature. After 24 hours, the moulds were demoulded and maintained at room temperature until a mechanical test was performed 28 days later. The mixture proportions of the geopolymer pastes containing micro- and nano-iron powders are given in Table 2.

2.2. Characterisation techniques

A Bruker D8 XRD instrument with a LYNXEYE detector was used to assess the mineral phases present in the raw materials and the geopolymers produced. CuKα radiation at 40 kV and 40 mA

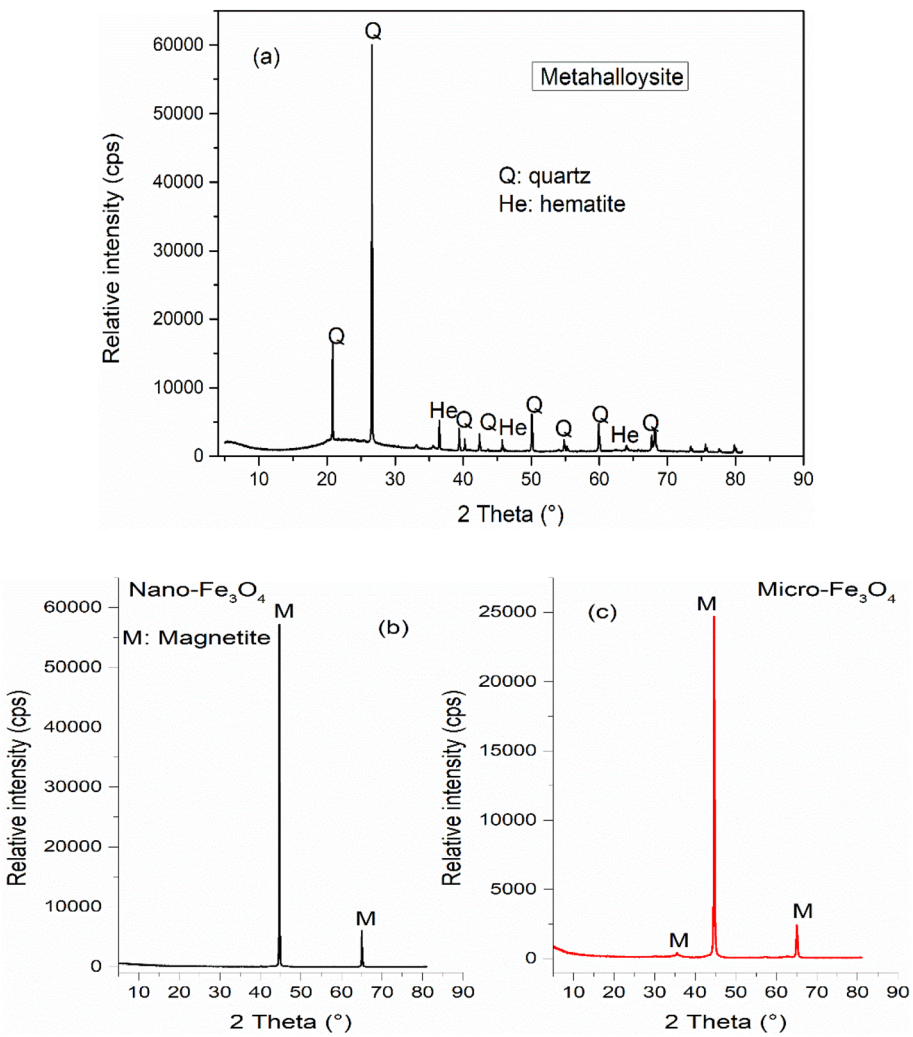

Fig. 1 X-ray patterns of metahalloysite (a), nano- (b) and micro-Fe_3O_4 powders (c).

was used to perform each measurement for 2 hours, with 2θ ranging from 5° to 80° in 0.03° steps.

The functional groups within raw materials and geopolymers were identified with a Bruker Vertex 80v infrared spectrometer using the KBr technique, the pellet from each sample was used for 32 scans at a resolution of 2 cm^{-1}. About 1.2 mg of the sample and 200 mg of KBr were combined to make each pellet.

The fresh geopolymer pastes were subjected to workability measurements immediately after mixing. A small cone with a bottom diameter of 38 mm, a top diameter of 19 mm, and a height of 57 mm was used for workability measurements, in accordance with previous research.[45,46]

Compressive strength was determined using hardened geopolymer paste cubes. Mechanical testing was performed with an Instron® 5965 universal testing machine under a constant displacement rate of 3 mm min^{-1}. The reported compressive strength, water absorption, porosity and bulk density values represent the average of five specimens tested for each geopolymer formulation. In addition, water absorption, apparent porosity, and bulk density were measured using an electronic balance (Sartorius, model 1712001) with a sensitivity of ±0.001 g, in accordance with the Archimedes principle. Prior to these measurements, the specimens were oven-dried at 40 °C until a constant mass was achieved.

3. Results and discussion

3.1. XRD and FTIR results

Fig. 1 presents the XRD patterns of metahalloysite (Fig. 1a), nano-Fe_3O_4 (Fig. 1b) and micro-Fe_3O_4 (Fig. 1c) powders. In the case of metahalloysite, the dominant mineral phases were quartz (SiO_2 PDF no. 00-046-1045) and hematite (Fe_2O_3 PDF no. 00-024-0072). Near these crystalline phases, a halo peak was observed between 15° and 35° in the 2-theta range. This halo peak indicates the formation of a reactive or amorphous phase upon heating at 700 °C. The formation of reactive amorphous phases during calcination plays a crucial role in geopolymerisation, as these phases readily dissolve in alkaline solution and provide the reactive silica and alumina species required for the formation of the geopolymer network. A similar hump has been previously reported in

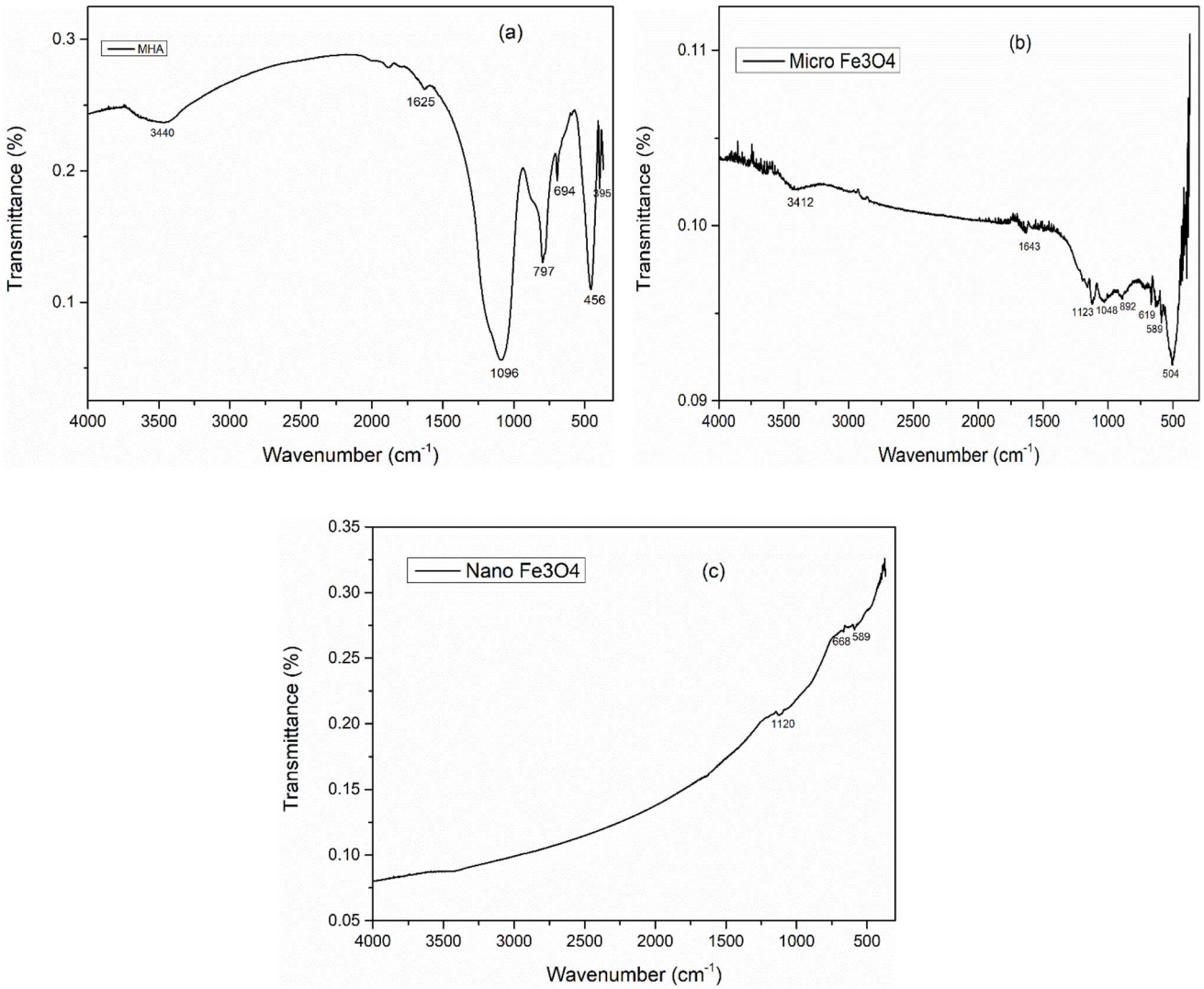

Fig. 2 Infrared spectra of calcined halloysite (a), micro (b) and nano (c) iron powders.

other thermally activated clays, such as kaolin[47] and tubular halloysite.[8] The iron powders exhibited reflection peaks of magnetite, indicating their purity. It should also be noted that the XRD patterns of the nano- and micro-Fe_3O_4 powders are very similar, indicating that both materials have the same magnetite crystalline phase, with the primary difference between them being particle size rather than phase composition.

Fig. 2 displays the FTIR spectra of calcined halloysite along with micro- or nano-iron materials. In the case of meta-halloysite powder, the broad band appearing at 3440 and 1625 cm^{-1} is assigned to vibrational modes of O–H belonging to the residual halloysite mineral.[9] The persistence of these absorption bands suggests that they are not fully transformed into metahalloysite. The broad absorption bands appearing at 1096 cm^{-1} are assigned to the asymmetric stretching band of Si–O–Al, attributable to the amorphous phase related to the transformation of halloysite mineral into metahalloysite.[8,48] The absorption bands located at 797, 694, 456 and 395 cm^{-1} are assigned to asymmetric stretching vibrations of Si–O related to quartz mineral.[49,50] For the iron powders, the absorption bands appearing at 3440 and 1625 cm^{-1} (Fig. 2b) are assigned to stretching bonds of surface water molecules or to an envelope formed by hydrogen-bonded surface OH groups.[51,52] The absorption bands at 1120, 1123, and 1048 cm^{-1} are assigned to C–O stretching vibrations (Fig. 2b and c).[53] Finally, the absorption bands at 797, 694, 668, 589, 456, and 395 cm^{-1} are assigned to the Fe–O stretching vibration mode (Fig. 2b and c).[54–56]

3.2. Fresh properties of geopolymer mixtures

The flow values for fresh geopolymer according to different procedure mixes are shown in Fig. 3. It is clear that the combined effects of powder type and mixing process significantly affected the flow performance of the mixtures. Regardless of the type of powder used, the inclusion of iron powder reduced the flow workability of the fresh geopolymer mixtures. This suggests that the addition of micro- and nano-Fe_3O_4 alters the microstructure of geopolymer pastes, thereby increasing viscosity. This is more evident in formulations that use the second mixing procedure, in which the iron particles are dissolved in an alkaline solution before being combined with the calcined halloysite powders. The breakdown of iron particles in alkaline solution would consume some of the latter, slowing the

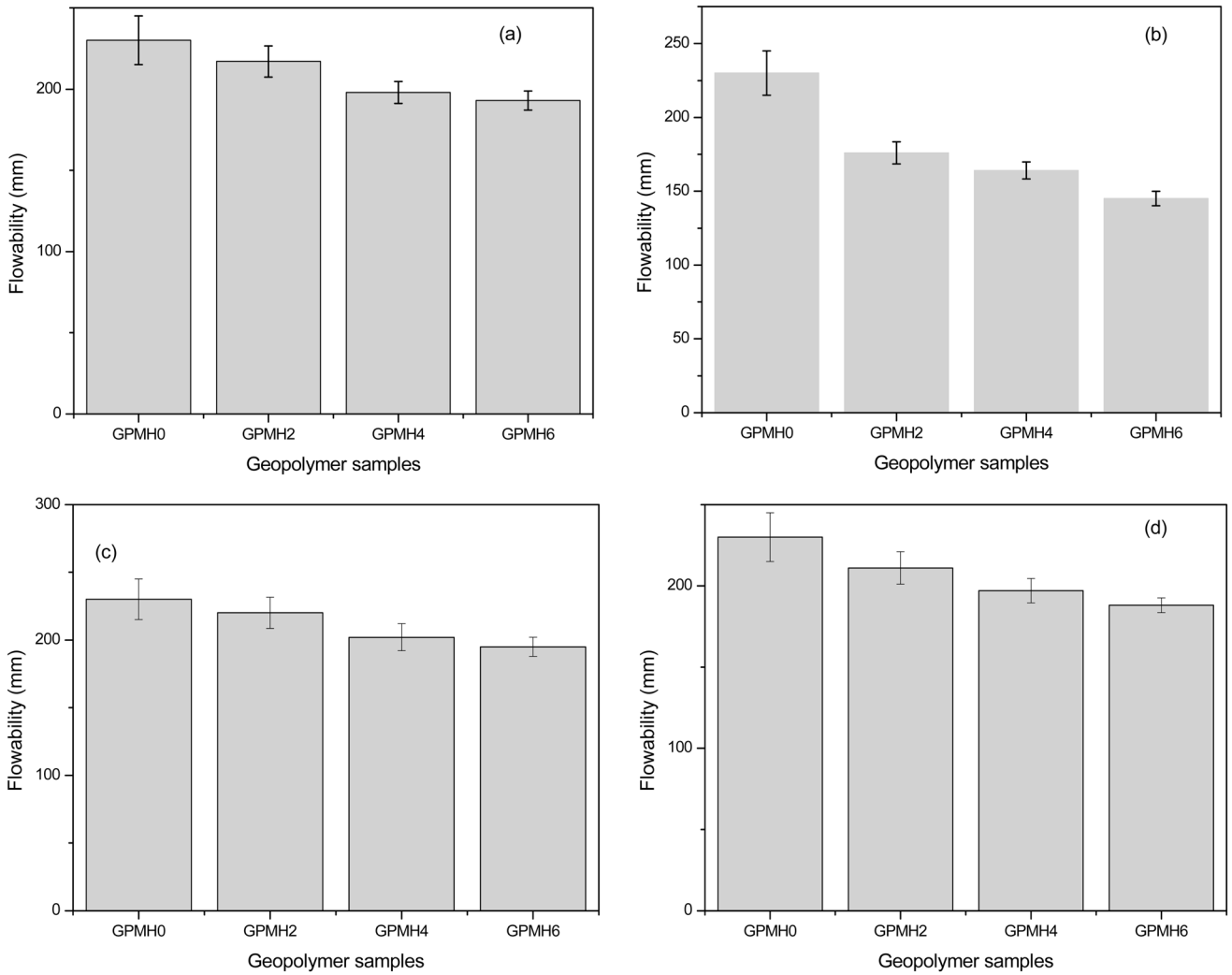

Fig. 3 Flow values of fresh geopolymer pastes blended with micro and nano iron powders applying procedure mix I (a and c) and II (b and d).

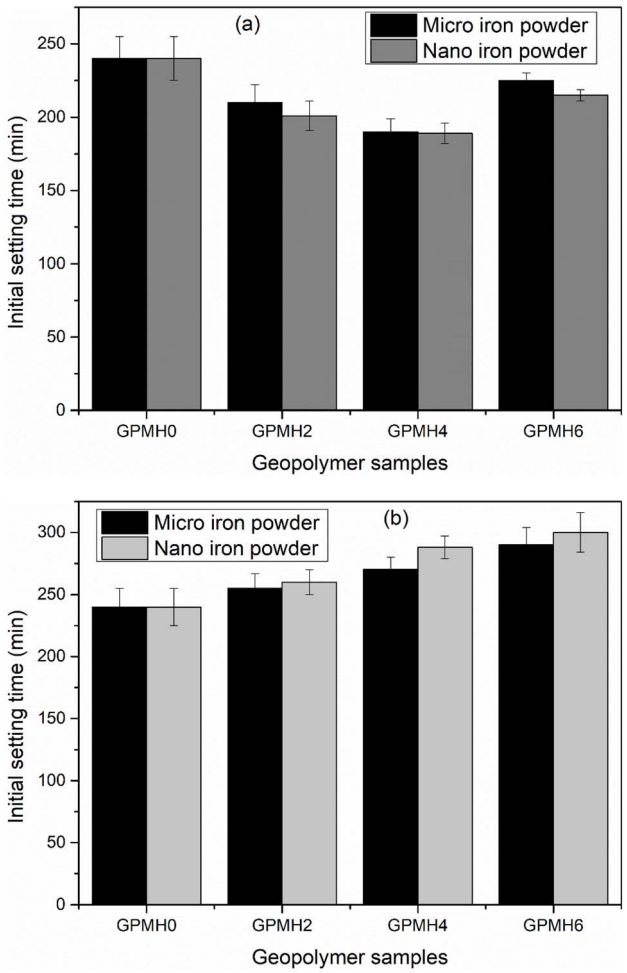

Fig. 4 Initial setting time of geopolymer binders blended with micro and nano iron powders using the first (a) and second (b) mix procedures.

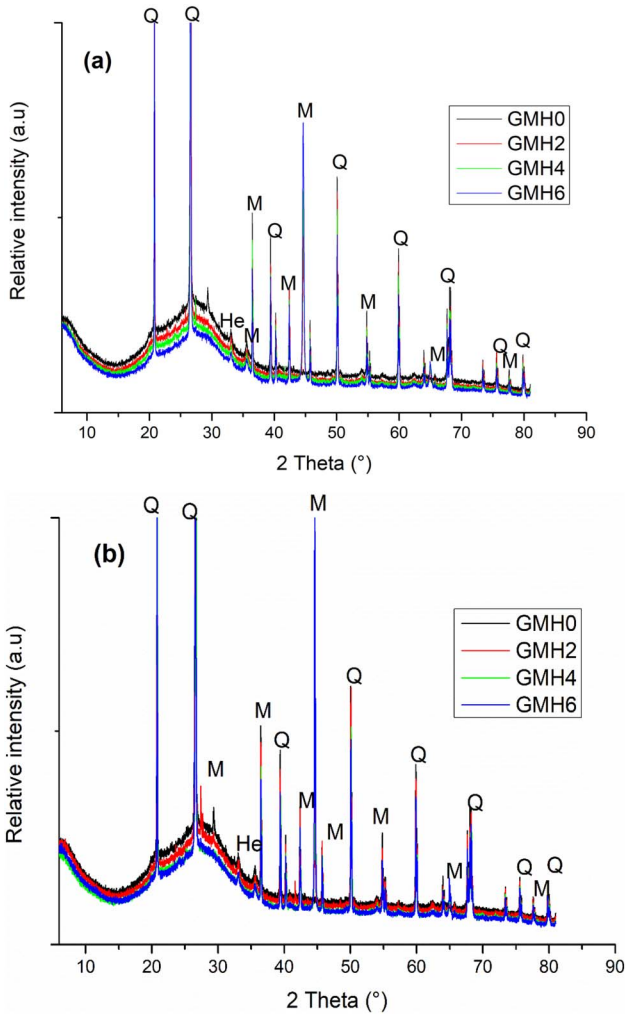

Fig. 5 X-ray patterns of geopolymer blended with micro (a) and nano (b) Fe_3O_4 powders.

solubility of calcined clay. The flow value decreased from 230 to 195 mm and from 230 to 188 mm, respectively, when adding micro- and nano-Fe_3O_4 powders using the first mixing procedure. In the second mix procedure, the values ranged from 230 to 150 mm and from 230 to 188 mm, respectively. This workability was likely due to the frictional effect of different iron powders on thermally activated halloysite in an alkaline medium. As a result, the workability of the different mixes decreased with the further increase in iron powder, consistent with other studies incorporating iron powder at different percentages.[38,57] Additionally, the roughness and fineness modulus of iron powders may have greatly enhanced the cohesion of geopolymer binder ingredients. This would have increased the solution demand in the mixture and reduced the flowability. Based on these above conclusions, the obtained results can be compared with those reported in literature.[43]

Fig. 4 presents the initial setting times recorded for a fresh metahalloysite-based geopolymer blended with micro- and nano-iron powders at varying dosages (0, 2, 4, and 6 wt%). For the first mixing procedure, the initial setting decreased from 240 to 225 min for samples blended with micro-iron powder and from 240 to 215 min for those blended with nano-iron powder. The reduced setting may be associated with possible interaction between iron species (*e.g.* Fe^{3+} and Fe^{2+}) and alkaline solution, which may react with HO^- to form $Fe(OH)_3$ and $Fe(OH)_2$ (eqn (2) and (3)). Furthermore, in the highly alkaline environment these iron hydroxides compounds can be dissolved to form FeO_2^- and FeO_2^{2-}, respectively thereby reducing the setting time. However, it should be noted the present study does not directly quantify Fe dissolution or speciation. Therefore, the role of Fe^{3+}/Fe^{2+} species in modifying the geopolymerisation kinetics should be considered as a potential mechanism rather than a confirmed reaction pathway. In samples incorporating the micro-iron powder with high particle size, the homogeneity of the geopolymer binder within the matrix was improved, accelerating setting and resulting in the lower setting time recorded. The increased initial observed in the second mixing procedure was likely due to the dissolution of both iron powders into the alkaline solution. Their dissolution reduced the alkaline and then affected the dissolution of calcined halloysite. In fact, the *in situ* dissolution of both iron powder types generated more nucleic sites in

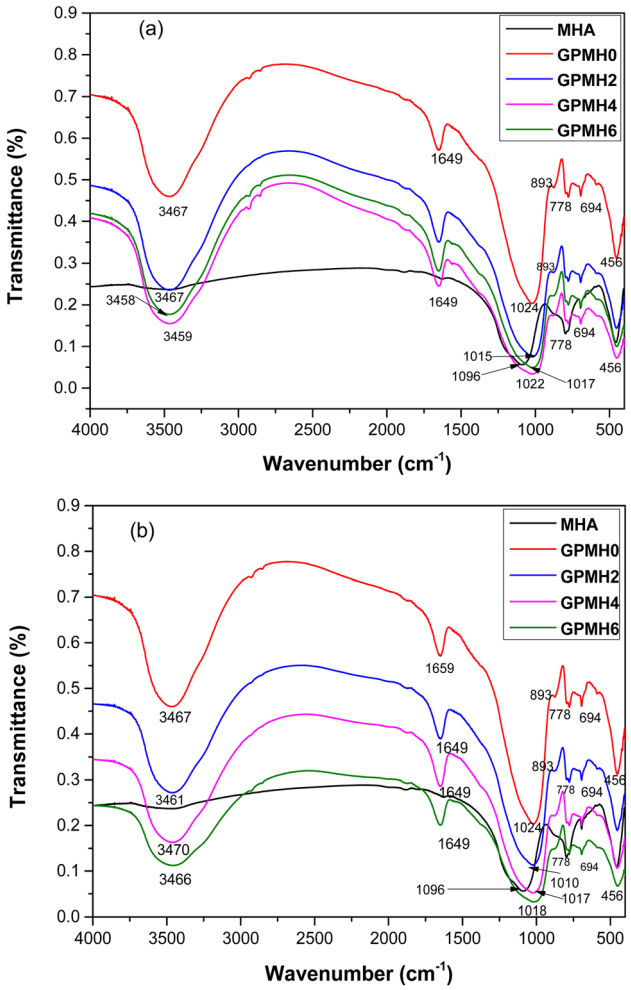

Fig. 6 Infrared spectra of calcined halloysite (MHA) and geopolymer blended with 2, 4 and 6 wt% of micro (a) and nano (b) iron powders.

different geopolymer mixtures, affecting the workability and progressively delaying the setting time. In addition, the slight increase recorded between GPMH4 and GPMH6 samples (Fig. 4a) might be attributed to the competitive environment created between the nano iron powders with metahalloysite. The nano iron powders in contact with the alkaline solution will release more iron with FeO_2^- and FeO_2^{2-} species in alkaline medium interacted with Na^+ to form $2NaFeO_2$ and Na_2FeO_2 compounds as described in eqn (1). This would limit the availability of Na^+ cations needed for balancing the negative charge within the geopolymer framework prolonging the setting time with a little longer condensation or polymerisation process. This adverse effect impeded the creation of long polymerization chains and augmented the pore diameter and shape of the final geopolymer material post-geopolymerization, hence diminishing its compressive strength development.

$$Fe_3O_4 + 4NaOH \rightarrow 2NaFeO_2 + Na_2FeO_2 + 2H_2O \quad (1)$$

$$Fe(OH)_3 + NaOH \rightarrow NaFeO_2 + 2H_2O \quad (2)$$

$$Fe(OH)_2 + 2NaOH \rightarrow Na_2FeO_2 + H_2O + H_2 \quad (3)$$

3.3. Phases evolution

Fig. 5 shows the XRD patterns of geopolymer blended with 0, 2, 4 and 6 wt% of micro- (Fig. 5a) and nano- (Fig. 5b) iron powders. It appears that the halo peak in thermally activated halloysite, located between 15° and 35° 2-theta, shifted to 20°–40° 2-theta on the geopolymer diffractograms of the GMH0, GMH2, GMH4, and GMH6 samples. This displacement is likely due to the geopolymerization reaction that occurs after mixing.[58] All the geopolymer specimens showed the same crystalline mineral phases (quartz (Q) and magnetite (M)) present in the solid precursor (thermally activated halloysite at 700 °C). This suggests that these mineral phases are inert or partially dissolved in alkaline medium during the geopolymerization reaction.[59] The intensity of the magnetite reflection peaks in the XRD patterns of the geopolymer samples slightly decreased with increasing magnetite content. In addition, the characteristic amorphous halo of geopolymers containing 2, 4, and 6 wt% iron powder was noticeably less pronounced than that of the reference sample (GMH0, without additive). This reduction in the amorphous phase intensity is consistent with the lower compressive strength observed for the mixture containing 6 wt% nano-iron powder (Fig. 5b). The presence of crystalline mineral phases within the geopolymer matrix can contribute to structural reinforcement by acting as micro-aggregates, as previously reported in ref. 60.

The FTIR spectra of calcined halloysite (MHA) and geopolymer blended with 0, 2, 4 and 6 wt% of micro and nano iron powders are shown in Fig. 6. It can be observed that the broad absorption bands at 1649, 3458, 3459, 3467, 3466, 3461, 3470, and 3473 cm^{-1} are assigned to stretching vibrations of water molecules within the geopolymer network.[61] The broad at 1096 cm^{-1} on MHA spectrum shifted towards lower frequency after alkaline action; 1024 cm^{-1}, 1015 cm^{-1}, 1017 cm^{-1} and 1022 cm^{-1} for GPMH0, GPMH2, GPMH4 and GPMH6 blended with micro iron powders at varied dosages (Fig. 6a). In case of geopolymer samples blended with nano iron powders this band shifted to 1010 cm^{-1}, 1017 cm^{-1} and 1018 cm^{-1}, respectively (Fig. 6b). This behaviour is likely attributed to stretching vibrations modes of Si–O–Al of geopolymer network.[49] The last bands observed at 778, 694, and 456 cm^{-1} are attributed to the stretching vibration modes of Si–O–Si, Si–O–Al, and Al–O.[62–64] Finally, the XRD and FTIR analyses did not point out any changes. This could be attributed to the milling effect of hardened geopolymer samples cured at 28 days which ground and sieved under 75 μm before running the measurement. Hence running these analyses *in situ* on the fresh geopolymer pastes blended with both iron powders should be hopeful for more clarity. Furthermore, XRD results also showed the reflection peaks of magnetite suggesting their none total dissolution which could act as inactive granular fillers through the presence of unreacted phases in geopolymer binder specimens as reported in ref. 40.

3.4. Mechanical properties

The 28-day compressive strength of geopolymers incorporating micro- and nano-iron powders, prepared using the first and second procedures, is presented in Fig. 7 and 8, respectively. For specimens produced using the first procedure, the

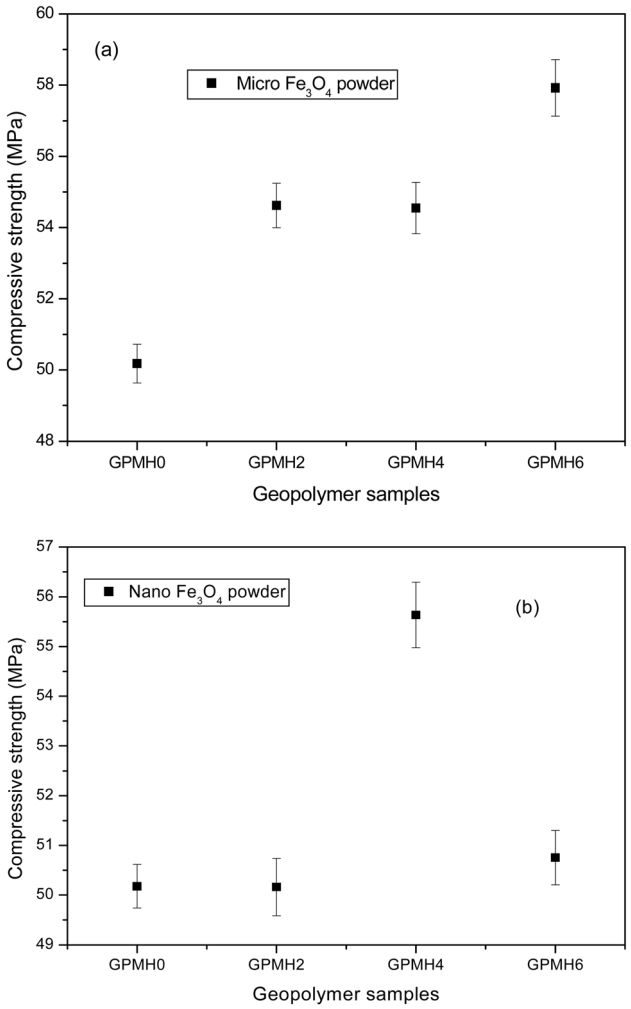

Fig. 7 Compressive strength recorded on geopolymer made with first procedure.

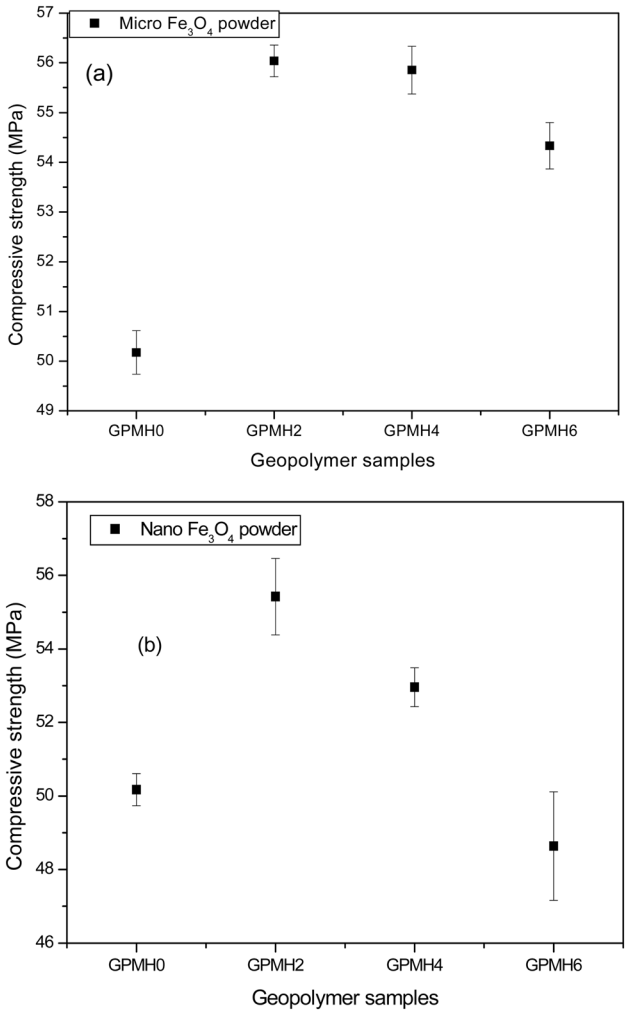

Fig. 8 Compressive strength recorded on geopolymer made with second procedure.

incorporation of 6 wt% micro-iron powder resulted in the highest compressive strength (57.92 MPa, Fig. 7a), while 4 wt% nano-iron powder yielded a strength of 55.42 MPa (Fig. 7b), both exceeding that of the control geopolymer without additive. The improved strength observed with micro-iron powder can be attributed to the relatively coarse particles acting as micro-aggregates, promoting better packing and enhanced homogenisation between the geopolymer gel and the solid constituents within the matrix. This contributes to improved connectivity and densification, leading to higher strength development. In the case of nano-iron powder, 4 wt% appears to be the optimum content for compressive strength enhancement. In addition, it noticed any changes when added 2 or 4% (Fig. 7a) of micro iron powder which is consistent with previous study where the authors replaced metakaolin with 2 and 4% of iron powder.[32] However, a deeply detailed microstructural and macrostructural study of geopolymer binders from these specimens is needed to establish such a phenomenon.

However, when the nano-iron powder content exceeded 4 wt% (Fig. 7b), a significant reduction in compressive strength was observed. This behaviour may be attributed to excessive iron species formed in the alkaline medium, which can interact with Na^+ ions and reduce their availability for balancing the negative charges within the geopolymer framework.[35] As a result, the condensation and polymerisation processes may be hindered, leading to the formation of a less compact matrix and consequently lower compressive strength.[36]

For specimens prepared using the second procedure (*in situ* mixing of the alkaline activator with micro- and nano-iron powders), the incorporation of 2 wt% micro-iron powder and 4 wt% nano-iron powder resulted in the highest compressive strengths of 56.03 MPa (Fig. 8a) and 55.63 MPa (Fig. 8b), respectively. This strength enhancement is consistent with previous studies suggesting the possible formation of iron–silicate interactions within geopolymer systems.[32,65,66] The reduction in strength observed beyond these optimum dosages might be associated with the excessive dissolution of iron powder under alkaline conditions, leading to an increased concentration of iron ions that can interfere with the geopolymerisation process and hinder the development of a well-connected aluminosilicate network. Furthermore, during the *in situ* mixing process, a portion of the alkaline activator could

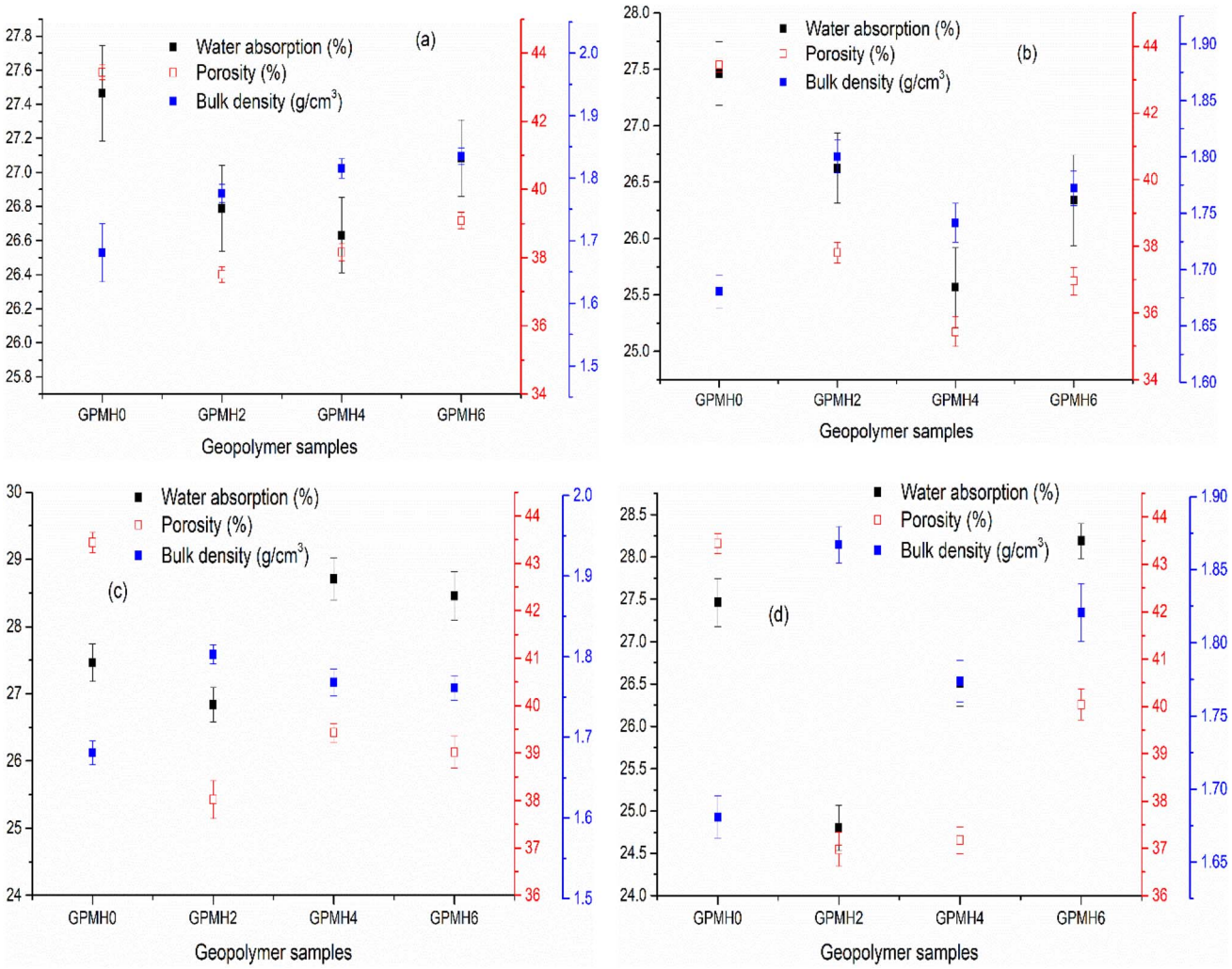

Fig. 9 Water absorption, porosity and bulk density values of metahalloysite based geopolymer composites blended with nano and micro Fe_3O_4 powder applying procedures I (a and b) and II (c and d).

be consumed through reactions with the iron particles, thereby limiting the effective dissolution of metahalloysite and negatively affecting strength development. It is worth noting that in the present study, the available characterisation techniques do not provide direct evidence of Fe incorporation into the geopolymer gel structure. Therefore, the observed improvement in mechanical performance may primarily arise from physical effects such as particle packing and micro-filler action, while potential chemical contributions of Fe species remain speculative and require further investigation.

Also, the results indicate that, at their optimum dosages, micro- and nano-iron particles act as reaction accelerators and micro-fillers, promoting a denser packing of the matrix and leading to the development of a strong and compact geopolymer structure.[67,68] The decrease in compressive strength (Fig. 8a and b) observed in geopolymer samples when added 4 and 6% of both iron powders in the second procedure could be attributed to the iron(II) dioxo ion, FeO_2^{2-} (eqn (3)) which is more pronounced in nano than micro powders. Finally, the release of H_2 during the premixing would provide the air bubbles as seen in the matrix, which are detrimental for the strength development, demonstrating the optimum at 2% of both iron powders added.

3.5. Water absorption, porosity and bulk density

Fig. 9 presents the water absorption, apparent porosity, and bulk density of metahalloysite-based geopolymer composites incorporating micro- and nano-iron powders at dosages of 0, 2, 4, and 6 wt%. For specimens prepared using the first procedure, water absorption decreased from 27.5% to 26.6% (Fig. 9a) and from 27.5% to 25.82% (Fig. 9b) with the addition of 2 wt% micro-iron powder and 4 wt% nano-iron powder, respectively. However, at higher iron contents, water absorption increased to approximately 27% and 28%, respectively. The initial reduction in water absorption suggests a pore-filling effect of iron particles, contributing to a denser and more compact geopolymer matrix. Correspondingly, the values of apparent porosity and bulk density ranged between 39–44% and 1.70–1.85 g cm^{-3} (Fig. 9a), and 35–44% and 1.68–1.82 g cm^{-3} (Fig. 9b), respectively. The observed increase in water absorption and porosity at

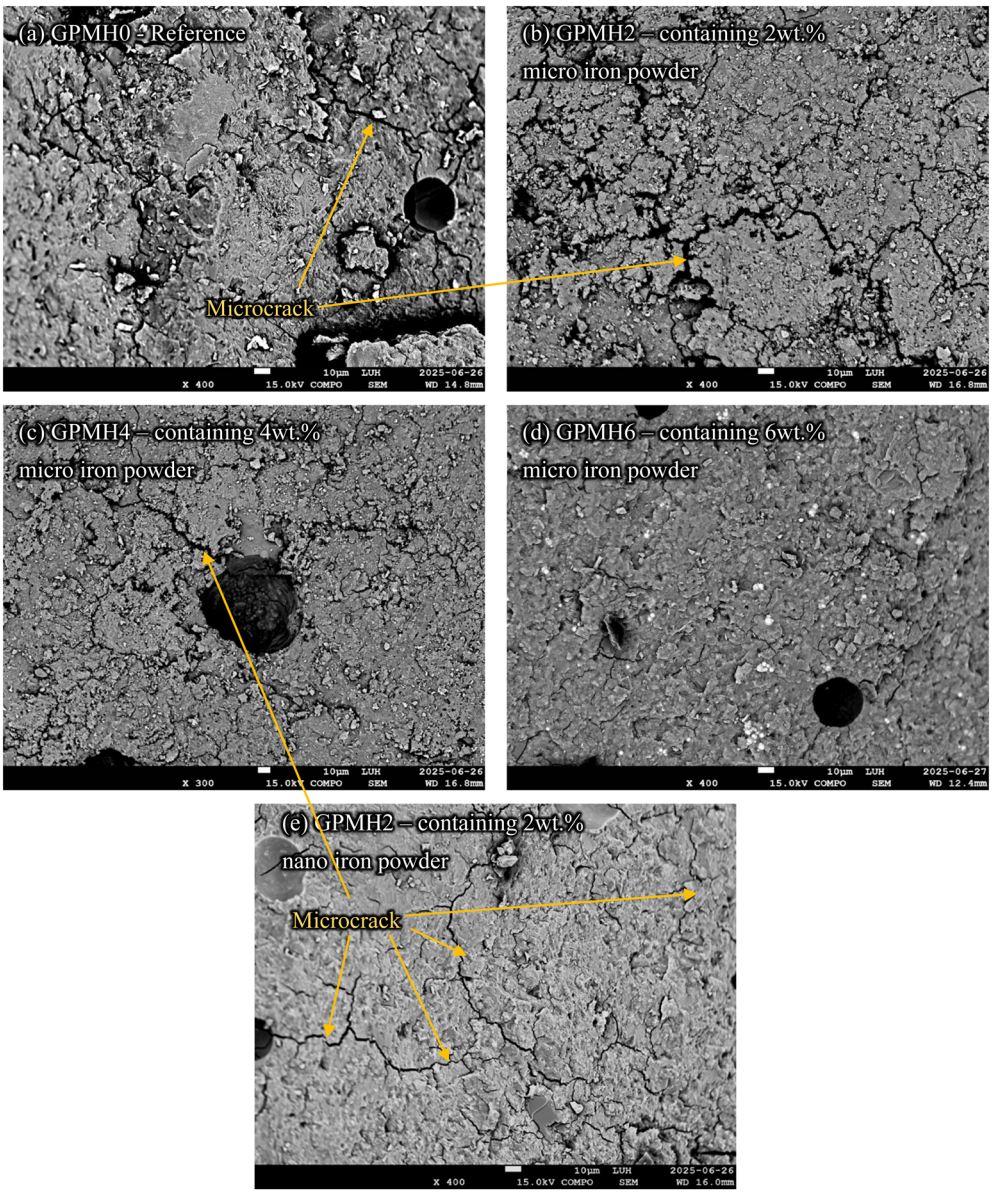

Fig. 10 SEM images (10 μm) of geopolymer blended with 0, 2, 4 and 6 wt% of micro iron powder (a–d) and nano-iron powder (e) from first procedure.

higher dosages is consistent with the trend in compressive strength, which decreased beyond the optimum iron content. Similar behaviour has been reported in the literature, where excessive incorporation of iron powder in cementitious systems adversely affects the development of mechanical properties due to increased pore connectivity within the matrix.[69,70]

For samples prepared using the second procedure (Fig. 9c), water absorption and apparent porosity ranged from 26.5–28.5% and 38.02–43.5%, respectively, for mixtures containing micro-iron powder. For those incorporating nano-iron powder (Fig. 9d), the corresponding ranges were 24.80–27.50% and 36.80–43.50%. The bulk densities obtained from both procedures were within a similar range of 1.68–1.82 g cm^{-3} and 1.68–1.83 g cm^{-3}, respectively. It is noteworthy that porosity and water absorption followed comparable trends and exhibited similar magnitudes regardless of the mixing procedure. However, iron dosages exceeding 4 wt% were found to be detrimental, as excess particles are unlikely to effectively participate in the geopolymerisation process. This leads to the formation of a less compact matrix with increased open voids and pore connectivity, which promotes higher water uptake during testing. Conversely, the incorporation of iron powder at optimum levels contributes to progressive matrix densification and reduced porosity. Previous studies also reported the increase in bulk density of hardened geopolymer binders with the increased iron powder from different sources.[35,39,71,72] These authors claimed that the increase in bulk density is owing to the filler effect of micro or nano iron powders used, resulting in densified geopolymer specimens with less open voids.

3.6. SEM analysis

Fig. 10 presents SEM micrographs of metahalloysite-based geopolymer binders incorporating micro- and nano-iron powders after 28 days of curing. As observed, the microstructures appear heterogeneous, characterised by the presence of some unreacted particles and minor microfissures. These features suggest an incomplete reaction of the calcined halloysite, while the incorporation of iron powders contributes to the formation of a comparatively denser and more compact matrix. For geopolymer samples prepared using the first procedure (*i.e.*, dry mixing metahalloysite with 2, 4, and 6 wt% micro-iron powder), the micrographs indicate reduced porosity and improved matrix densification compared with those incorporating nano-iron powder. This observation is consistent with the compressive strength development. In contrast, the geopolymer sample containing 6 wt% nano-iron powder (Fig. 10e) exhibits extensive microcracking within the matrix, which correlates with the lower compressive strength observed at this dosage. This microcracking may be associated heat release associated with the exothermic reactions occurring during the dissolution and oxidation of nano-iron particles in the alkaline medium, as reported in previous studies.[73] The exothermic reactions occurring during the dissolution of nano-iron particles generated air bubbles that were difficult to eliminate, leading to the formation of open voids and pores within the geopolymer matrix and consequently reducing strength development. In contrast, the progressive densification observed in samples containing micro-iron powder correlates well with the measured strength improvement. This behaviour can be attributed to the larger particle size and lower dissolution rate

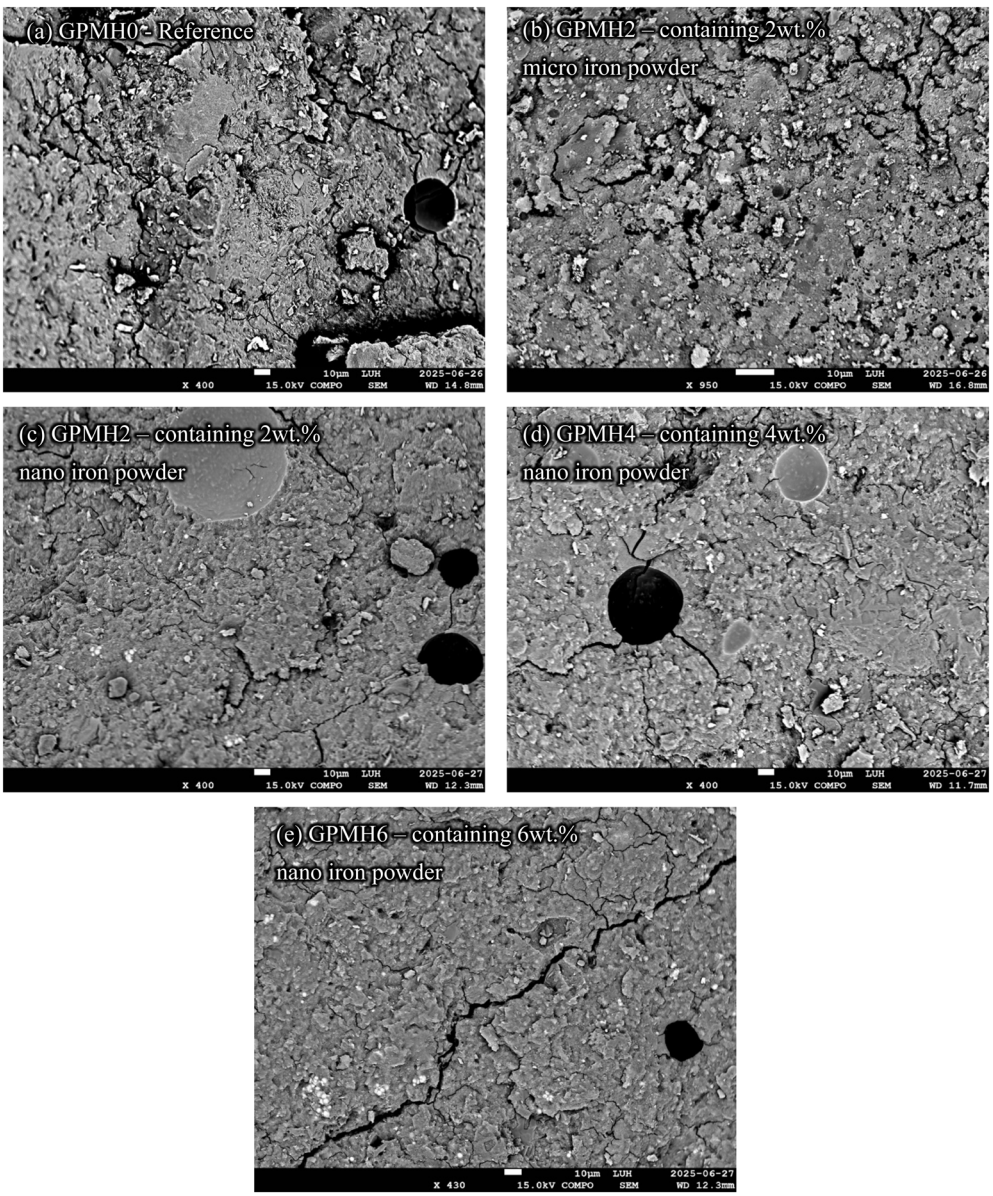

Fig. 11 SEM images (10 μm) of geopolymer blended with 0, 2, 4 and 6 wt% of micro iron powder (a–d) and nano-iron powder (e) from the second procedure.

of micro-iron particles in the alkaline medium, which enables them to act as effective pore fillers and contribute to reinforcement of the geopolymer structure.

Fig. 11 presents SEM micrographs of reference geopolymer mixture (Fig. 11a) along with those made using micro- (Fig. 11b) and nano-iron powders (Fig. 11c–e) at various dosages, prepared using the second procedure in which the iron powders were first dispersed in the alkaline activator prior to the addition of calcined halloysite. The microstructures appear more homogeneous in samples containing nano-iron powder than in those with micro-iron powder, indicating the higher dissolution rate of nano-sized particles in the alkaline medium. The pre-dissolution of iron powders in the alkaline solution promotes improved dispersion within the geopolymer matrix and enhances cohesion between the reaction products. As mentioned in the foregoing, observed improvement in the binder matrix may be attributed to a combination of mechanisms. One possible contribution is the formation of iron–silicate (ferri-/ferro-silicate) interactions within the geopolymer matrix, which could contribute to matrix reinforcement and improved mechanical performance. In addition, the fine particle size of the iron powders may also promote a packing or filler effect, leading to a denser binder matrix. Further studies using advanced characterization techniques would be required to confirm the relative contribution of these mechanisms. However, iron contents beyond the optimum level were found to be detrimental to strength development. This can be attributed to excessive consumption of the alkaline activator by the dissolved iron species, leaving insufficient alkalinity to effectively dissolve the calcined halloysite. As a result, a less compact and poorly densified structure is formed.

At an addition level of 2 wt% for both micro- and nano-iron powders, the micrographs reveal the presence of numerous nucleation sites favourable for geopolymerisation, promoting enhanced polycondensation between Al, Si, and Fe species and resulting in a stronger matrix (Fig. 11b and c). In contrast, higher dosages led to the appearance of microfissures and pores within the matrix (Fig. 11d and e), consistent with the observed reduction in compressive strength.

4. Conclusion

The present study investigated the influence of two mixing procedures comprising procedure I (dry blending of metahalloysite with iron powder followed by the addition of the alkaline activator) and procedure II (pre-dispersion of iron powder in the alkaline activator followed by metahalloysite addition), on the fresh and hardened properties of metahalloysite-based geopolymers incorporating micro- and nano-iron powders at dosages of 0, 2, 4, and 6 wt%. The following conclusions can be drawn:

• Flowability decreased with increasing iron powder content due to the associated rise in mixture viscosity.

• Under procedure I, the incorporation of micro-iron powder up to 6 wt% resulted in the highest compressive strength (57.92 MPa), outperforming nano-iron powder. This behaviour is attributed to the filler effect of the coarser particles, which enhances matrix densification.

• Under procedure II, the addition of 2 wt% of either micro- or nano-iron powder provided the most favourable matrix cohesion and strength development.

• Iron powder contents exceeding the optimum level (2 wt% for procedure II) were detrimental to strength, primarily due to reduced workability and excessive consumption of the alkaline activator, which limited effective geopolymerisation.

• Geopolymers produced using procedure II consistently achieved compressive strengths above 40 MPa, indicating their suitability for structural and engineering applications.

• SEM observations confirmed that samples incorporating iron powders exhibited a more compact and densified microstructure compared with the reference geopolymer, with the degree of densification strongly influenced by the mixing procedure.

• Overall, both micro- and nano-iron powders can be effectively utilised at low dosages to enhance the performance of metahalloysite-based geopolymer binders, provided that the mixing procedure and iron content are carefully optimised to avoid adverse effects on geopolymerisation and strength development.

• The final products developed compressive strengths exceeding 48 MPa, indicating their potential use as construction materials for engineering applications such as road pavements and building components, while aligning with sustainable construction principles by reducing reliance on energy-intensive cement production.

Notwithstanding the enhanced performance of the developed geopolymer composites, further investigation using advanced spectroscopic techniques such as XPS, Mössbauer spectroscopy, SEM-EDS mapping, or ICP-OES would be required to directly determine the dissolution behaviour of Fe species and their possible incorporation into the geopolymer gel phase.

Conflicts of interest

There are no conflicts to declare.

Data availability

The datasets generated and/or analysed during the current study are available from the corresponding author upon request.

Acknowledgements

Rodrigue Cyriaque Kaze gratefully acknowledges the financial support of the Jean D'Alembert Junior Fellowship for 2023–2025 for his stay in LMPS, ENS Université Paris Saclay. This work has been supported as part of the France 2030 Program ANR-11-IDEX-0003.

References

1 N. Ranjbar, *et al.*, Hardening evolution of geopolymers from setting to equilibrium: A review, *Cem. Concr. Compos.*, 2020, **114**, 103729.

2 A. Naghizadeh, *et al.*, Re-activation of recycled fly ash-based geopolymer binder to enhance mechanical properties, *Case Stud. Constr. Mater.*, 2025, e04967.
3 A. Naghizadeh, *et al.*, Effective recycled binder produced upon thermal activation to enhance mechanical properties of fly ash-based geopolymer mortars, *Dev. Built Environ.*, 2025, 100688.
4 A. Naghizadeh, *et al.*, Circular production of recycled binder from fly ash-based geopolymer concrete, *Constr. Build. Mater.*, 2024, **415**, 135098.
5 J. Davidovits, Chemistry of geopolymeric systems terminology, in *Proceedings of Geopolymer*, 1999, vol. 99, pp. 9–39.
6 J. N. Y. Djobo, D. Stephan and A. Elimbi, Setting and hardening behavior of volcanic ash phosphate cement, *J. Build. Eng.*, 2020, **31**, 101427.
7 C. R. Kaze, *et al.*, Reaction kinetics and rheological behaviour of meta-halloysite based geopolymer cured at room temperature: Effect of thermal activation on physicochemical and microstructural properties, *Appl. Clay Sci.*, 2020, **196**, 105773.
8 N. Ranjbar, *et al.*, Halloysite reinforced 3D-printable geopolymers, *Cem. Concr. Compos.*, 2023, **136**, 104894.
9 B. Zhang, *et al.*, Effect of the SiO_2/Al_2O_3 Molar Ratio on the Microstructure and Properties of Clay-based Geopolymers: A Comparative Study of Kaolinite-based and Halloysite-based Geopolymers, *Clays Clay Miner.*, 2022, **70**(6), 882–902.
10 Z. Zhang, *et al.*, Effects of halloysite in kaolin on the formation and properties of geopolymers, *Cem. Concr. Compos.*, 2012, **34**(5), 709–715.
11 C. R. Kaze, *et al.*, Reactivity and mechanical performance of geopolymer binders from metakaolin/meta-halloysite blends, *Constr. Build. Mater.*, 2022, **336**, 127546.
12 V. Zivica, M. T. Palou and T. I. Ľ. Bágeľ, High strength metahalloysite based geopolymer, *Composites, Part B*, 2014, **57**, 155–165.
13 B. Zhang, *et al.*, Effect of curing conditions on the microstructure and mechanical performance of geopolymers derived from nanosized tubular halloysite, *Constr. Build. Mater.*, 2021, **268**, 121186.
14 B. Zhang, *et al.*, Geopolymerization of halloysite via alkali-activation: Dependence of microstructures on precalcination, *Appl. Clay Sci.*, 2020, **185**, 105375.
15 C. Rodrigue Kaze, *et al.*, Characterization, reactivity and rheological behaviour of metakaolin and Meta-halloysite based geopolymer binders, *Cleaner Mater.*, 2021, **2**, 100025.
16 B. Zhang, *et al.*, Novel acid-based geopolymer synthesized from nanosized tubular halloysite: The role of precalcination temperature and phosphoric acid concentration, *Cem. Concr. Compos.*, 2020, **110**, 103601.
17 L. Deng, *et al.*, Effects of calcination and acid treatment on improving benzene adsorption performance of halloysite, *Appl. Clay Sci.*, 2019, **181**, 105240.
18 T. Yu, *et al.*, Calcined nanosized tubular halloysite for the preparation of limestone calcined clay cement (LC^3), *Appl. Clay Sci.*, 2023, **232**, 106795.
19 S. Paruthi, *et al.*, A comprehensive review of nano materials in geopolymer concrete: Impact on properties and performance, *Dev. Built Environ.*, 2023, **16**, 100287.
20 A. Drabczyk, *et al.*, Review of Geopolymer Nanocomposites: Novel Materials for Sustainable Development, *Materials*, 2023, **16**, 3478.
21 N. Veeramani, *et al.*, Effects of polymeric microcapsules on self-healing composites reinforced with carbon fibers: a comparative study, *Int. Polym. Process.*, 2023, **38**(4), 483–495.
22 Z. Su, W. Hou and Z. Sun, Recent advances in carbon nanotube-geopolymer composite, *Constr. Build. Mater.*, 2020, **252**, 118940.
23 N. Veeramani, *et al.*, Investigation of microcapsules based self-healing composites embedded with carbon nanotubes for improved healing efficiency, *J. Polym. Res.*, 2024, **31**(10), 312.
24 H. Mohamed, *et al.*, Mechanical and microstructural properties of geopolymer mortars from meta-halloysite: effect of titanium dioxide TiO_2 (anatase and rutile) content, *SN Appl. Sci.*, 2020, **2**(9), 1573.
25 J. Huang, *et al.*, A multi-scale study of enhancing mechanical property in ultra-high performance concrete by steel-fiber@nano-silica, *Constr. Build. Mater.*, 2022, **342**, 128069.
26 Z. Zidi, *et al.*, Synthesis of nano-alumina and their effect on structure, mechanical and thermal properties of geopolymer, *J. Asian Ceram. Soc.*, 2019, **7**(4), 524–535.
27 B. N. Bayiha, *et al.*, Effect of limestone dosages on some properties of geopolymer from thermally activated halloysite, *Constr. Build. Mater.*, 2019, **217**, 28–35.
28 P. Chindaprasirt, *et al.*, Effect of SiO_2 and Al_2O_3 on the setting and hardening of high calcium fly ash-based geopolymer systems, *J. Mater. Sci.*, 2012, **47**(12), 4876–4883.
29 T. Nongnuang, *et al.*, Characteristics of Waste Iron Powder as a Fine Filler in a High-Calcium Fly Ash Geopolymer, *Materials*, 2021, **14**(10), 2515.
30 M. L. Khouadjia, *et al.*, Sustainable Geopolymer Tuff Composites Utilizing Iron Powder Waste: Rheological and Mechanical Performance Evaluation, *Sustainability*, 2025, **17**(3), 1240.
31 K. Prałat, *et al.*, Determination of the Thermal Parameters of Geopolymers Modified with Iron Powder, *Polymers*, 2022, **14**(10), 2009.
32 X. Wu, *et al.*, Behavior of hematite, magnetite, and reduced iron powder in geopolymers: Effects of mechanical properties and reaction mechanism, *J. Cleaner Prod.*, 2024, **444**, 141178.
33 F. K. Tazune, *et al.*, Behavior of amorphous ferrisilicates with low weight concentration in ferric ions on the properties of metakaolin-based geopolymers, *Open Ceram.*, 2025, **24**, 100860.
34 D. L. V. Ngnintedem, *et al.*, Effects of Incorporating Ferric Ions from Hematite into Metakaolin on Microscopic Pore Structures and Compressive Strength of Geopolymers, *J. Mater. Eng. Perform.*, 2026, **35**(9), 8323–8346.
35 M. L. Khouadjia, *et al.*, Sustainable Geopolymer Tuff Composites Utilizing Iron Powder Waste: Rheological and Mechanical Performance Evaluation, *Sustainability*, 2025, **17**, 1240.

36 D. L. Ngnintedem, *et al.*, Effects of Iron Minerals on the Compressive Strengths and Microstructural Properties of Metakaolin-Based Geopolymer Materials, *Gels*, 2022, **8**, 525.
37 F. K. Tazune, *et al.*, Effects of Fe_2O_3/SiO_2 Molar Ratios in the Fe-Silica on the Compressive Strengths and Microstructural Properties of Geopolymer Materials Derived from Waste Fired Clay Brick and Metakaolin, *J. Inorg. Organomet. Polym. Mater.*, 2024, **34**(4), 1725–1737.
38 Z. Funda Akbulut, S. Guler and M. Khan, The effects of waste iron powder and steel fiber on the physical and mechanical properties of geopolymer mortars exposed to high temperatures, *Structures*, 2023, **58**, 105398.
39 T. Nongnuang, *et al.*, Characteristics of Waste Iron Powder as a Fine Filler in a High-Calcium Fly Ash Geopolymer, *Materials*, 2021, **14**(10), 2515.
40 M. Kaya, *et al.*, Influence of micro Fe_2O_3 and MgO on the physical and mechanical properties of the zeolite and kaolin based geopolymer mortar, *J. Build. Eng.*, 2022, **52**, 104443.
41 P. Duan, *et al.*, Fresh properties, compressive strength and microstructure of fly ash geopolymer paste blended with iron ore tailing under thermal cycle, *Constr. Build. Mater.*, 2016, **118**, 76–88.
42 S. C. Choi and W. K. Lee, Effect of Fe_2O_3 on the Physical Property of Geopolymer Paste, *Adv. Mater. Res.*, 2012, **586**, 126–129.
43 M. F. A. Abdu, Utilizing of iron filings in geopolymer mortar as a target for climate change mitigation, *Sustainable Chem. Pharm.*, 2025, **43**, 101910.
44 L. N. Ebongue, *et al.*, Effect of partial replacement of volcanic ashes by waste iron powder on the properties of phosphate inorganic polymers, *Discover Appl. Sci.*, 2024, **6**(4), 155.
45 A. M. Rashad, Influence of different additives on the properties of sodium sulfate activated slag, *Constr. Build. Mater.*, 2015, **79**, 379–389.
46 C. R. Kaze, *et al.*, Influence of mineralogy and activator type on the rheology behaviour and setting time of laterite based geopolymer paste, *Cem. Concr. Compos.*, 2022, **126**, 104345.
47 V. Pommer, *et al.*, Performance of thermally activated lower-grade clays – The impact of phase composition, *J. Build. Eng.*, 2025, **106**, 112685.
48 A. Lo Bianco, *et al.*, Geopolymerization of halloysite clay nanotubes mixed with hydroxypropyl cellulose for development of composite films with flame resistance properties, *Ceram. Int.*, 2025, 1–9.
49 A. Filipponi, *et al.*, Preparation and characterization of metakaolin-based geopolymer membrane supports by facile pressed one-part route, *Ceram. Int.*, 2023, **49**(4), 6834–6842.
50 J. N. Y. Djobo, *et al.*, Mechanical activation of volcanic ash for geopolymer synthesis: effect on reaction kinetics, gel characteristics, physical and mechanical properties, *RSC Adv.*, 2016, **6**(45), 39106–39117.
51 M. Gotić and S. Musić, Mössbauer, FT-IR and FE SEM investigation of iron oxides precipitated from $FeSO_4$ solutions, *J. Mol. Struct.*, 2007, **834–836**, 445–453.
52 M. Stoia, R. Istratie and C. Păcurariu, Investigation of magnetite nanoparticles stability in air by thermal analysis and FTIR spectroscopy, *J. Therm. Anal. Calorim.*, 2016, **125**(3), 1185–1198.
53 T. Q. Bui, *et al.*, Size-dependent magnetic responsiveness of magnetite nanoparticles synthesised by co-precipitation and solvothermal methods, *J. Sci.: Adv. Mater. Devices*, 2018, **3**(1), 107–112.
54 T. Girardet, *et al.*, Determination of the percentage of magnetite in iron oxide nanoparticles: A comparison between Mössbauer spectroscopy and Raman spectroscopy, *Solid State Sci.*, 2023, **143**, 107258.
55 S. Singh, *et al.*, Role of iron in the enhanced reactivity of pulverized Red mud: Analysis by Mössbauer spectroscopy and FTIR spectroscopy, *Case Stud. Constr. Mater.*, 2019, **11**, e00266.
56 A. Santos, *et al.*, Mechanical and thermal properties of geopolymers derived from metakaolin with iron mine waste, *Appl. Clay Sci.*, 2024, **258**, 107452.
57 S. J. Alserai, W. K. Alsaraj and Z. W. Abass, Effect of Iron Filings on the Mechanical Properties of Different Types of Sustainable Concrete, *Open Civ. Eng. J.*, 2018, **12**, 441–457.
58 S. Tome, *et al.*, Mineralogical evolution of raw materials transformed to geopolymer materials: A review, *Ceram. Int.*, 2024, **50**(19, part B), 35855–35868.
59 A. Elimbi, H. K. Tchakoute and D. Njopwouo, Effects of calcination temperature of kaolinite clays on the properties of geopolymer cements, *Constr. Build. Mater.*, 2011, **25**(6), 2805–2812.
60 H. K. Tchakoute, *et al.*, Influence of gibbsite and quartz in kaolin on the properties of metakaolin-based geopolymer cements, *Appl. Clay Sci.*, 2015, **107**, 188–194.
61 M. A. Mahrous, *et al.*, Investigating irradiation effects on metakaolin-based geopolymer, *Constr. Build. Mater.*, 2024, **437**, 136837.
62 B. Gopalakrishna and P. Dinakar, An innovative approach to fly ash-based geopolymer concrete mix design: Utilizing 100% recycled aggregates, *Structures*, 2024, **66**, 106819.
63 B. B. Jindal, *et al.*, Geopolymer concrete with metakaolin for sustainability: a comprehensive review on raw material's properties, synthesis, performance, and potential application, *Environ. Sci. Pollut. Res.*, 2023, **30**(10), 25299–25324.
64 C. R. Kaze, *et al.*, Development of alkali-activated composites from calcined iron-rich laterite soil, *Materialia*, 2021, **15**, 101032.
65 J. Davidovits and R. Davidovits, *Ferro-Sialate Geopolymers (-Fe-O-Si-O-Al-O-)*, Geopolymer Institute Library, 2020.
66 W. Zailani, *et al.*, Effect of iron oxide (Fe_2O_3) on the properties of fly ash based geopolymer, *IOP Conf. Ser.: Mater. Sci. Eng.*, 2020, **877**, 012017.
67 P. Kongsat, *et al.*, Effect of Morphologically Controlled Hematite Nanoparticles on the Properties of Fly Ash Blended Cement, *Nanomaterials*, 2021, **11**, 1003.
68 J. Zeng, *et al.*, Mechanics and microstructure analysis of geopolymer utilizing ilmenite tailing and metakaolin

powder as alkali-activated materials, *Case Stud. Constr. Mater.*, 2024, **21**, e03567.

69 P. N. Lemougna, *et al.*, The role of iron in the formation of inorganic polymers (geopolymers) from volcanic ash: a ^{57}Fe Mössbauer spectroscopy study, *J. Mater. Sci.*, 2013, **48**(15), 5280–5286.

70 X. Li, *et al.*, Effect of Fe^{2+}/Fe^{3+} on high-strength ceramsite prepared by sintering geopolymers using iron ore tailings, *Ceram. Int.*, 2022, **48**(4), 5681–5688.

71 T. Nongnuang, *et al.*, Characteristics of Waste Iron Powder as a Fine Filler in a High-Calcium Fly Ash Geopolymer, *Materials*, 2021, **14**, 2515.

72 K. Prałat, *et al.*, Determination of the Thermal Parameters of Geopolymers Modified with Iron Powder, *Polymers*, 2022, **14**, 2009.

73 J. Ren, *et al.*, Understanding the effects of hematite and brucite additions on fresh- and hardened-state properties of metakaolin-based geopolymer cements, *Appl. Clay Sci.*, 2025, **276**, 107932.